Journal of Materials Chemistry B

PAPER

Cite this: J. Mater. Chem. B, 2015, 3, 5760

Electrospun poly(L-lactide-co-caprolactone)–collagen–chitosan vascular graft in a canine femoral artery model†

Tong Wu,‡[a] Bojie Jiang,‡[b] Yuanfei Wang,[c] Anlin Yin,[a] Chen Huang,[a] Sheng Wang*[b] and Xiumei Mo*[a]

Received 2nd April 2015,
Accepted 4th June 2015

DOI: 10.1039/c5tb00599j

www.rsc.org/MaterialsB

Poly(L-lactide-*co*-caprolactone)–collagen–chitosan (P(LLA-CL)–COL–CS) composite grafts were electrospun in this study. Based on the test results for mechanical properties, biodegradability and *in vitro* cellular compatibility, the optimal weight ratio of P(LLA-CL) to COL/CS was set as 3 : 1. *In vivo* study was further performed in a canine femoral artery model. The results showed that the 3 : 1 grafts possessed excellent structural integrity, higher patency rate, better endothelial cell (EC) and smooth muscle cells (SMC) growth, as well as higher levels of gene and protein expression of angiogenesis-related cues than those of grafts based on P(LLA-CL). The findings confirmed that the addition of natural materials, such as collagen and chitosan, could effectively improve endothelialization, SMC incursion into the tunica media, and vascular remodeling for tissue engineering.

1. Introduction

The applications of the synthetic vascular grafts are often limited when the inside diameter of the graft is smaller than 5 mm, because of recurrent thrombosis and occlusion.[1] When compared to autografts, the lack of endothelialization of synthetic grafts often results in low patency rates, especially for long-term periods.[2] Thus, the idea of combining different structures and materials to construct multicomponent tissue-engineered vascular scaffolds for improved mechanical properties and biocompatibility has been intensively exploited.[3–6] Zhang[7] and Han[6] developed the dual-delivery of VEGF and PDGF by double-layered electrospun membranes for blood vessel regeneration, which synergistically promoted the development of VECs and VSMCs on the lumen and exterior of vascular grafts, respectively. The specially prepared multilayered fibrous scaffold could benefit blood vessel reconstruction. Yao[8] improved the PCL–chitosan hybrid small-diameter vascular grafts with sustained heparin release. The evaluation confirmed that the grafts enhanced the anti-thrombogenic properties and endothelialization. Fu[9] prepared electrospun gelatin–PCL and collagen–PLCL scaffolds and evaluated the applicability for vascular tissue engineering. It is proved that nanofibrous collagen–PLCL membranes with favorable mechanical and biological properties were desirable for vascular tissue engineering.

Therefore, an ideal small-diameter vascular graft should have two main advantages: scaffolds-based advantage and cell-based advantage. The first advantage means that it can provide advantages of both biological and synthetic materials to determine the outcomes of natural morphology and architectures, suitable mechanical properties, improved biocompatibility, and matched biodegradability.[3] As for the second advantage, it is expected that fast endothelialisation and SMC development, as well as high patency rates, can be promoted by adding growth factors (*e.g.* vascular endothelial growth factors, platelet-derived growth factor-bb, and fibroblast growth factor),[7,10] peptides derived from adhesion proteins, or extracellular matrix (ECM) molecules, including collagen, fibronectin, and polysaccharide.[11–13] Electrospinning has emerged as a popular technique to fabricate nanofibrous scaffolds for vascular reconstruction due to the simulation of the microstructure in native arteries and the availability of integration between grafts and surrounding cells and tissues.[2,11,14–16] In addition, it is convenient to adopt natural biomaterials as raw materials during the electrospinning process, and regulatory growth factors or anticoagulants (*e.g.* heparin and hirudin) can also be easily incorporated into the grafts.[8,11,17,18]

[a] State Key Laboratory for Modification of Chemical Fibers and Polymer Materials, College of Chemistry, Chemical Engineering and Biotechnology, Donghua University, Shanghai 201620, China. E-mail: xmm@dhu.edu.cn; Tel: +86 021 67792653

[b] Department of Emergency and Critical Care Medicine, Shanghai Tenth People's Hospital, Tongji University, Shanghai 200072, China. E-mail: wangsheng@tongji.edu.cn

[c] State Key Laboratory of Bioreactor Engineering, School of Resources and Environmental Engineering, East China University of Science and Technology, Shanghai 200237, China

† Electronic supplementary information (ESI) available. See DOI: 10.1039/c5tb00599j

‡ Tong Wu and Bojie Jiang contributed equally to this paper.

The antithrombotic performances of heparin release and endothelialization on the luminal surface were most intensively studied.[8,19–22] Heparin functions in the early periods after implantation, while long-term patency mainly depends on rapid endothelialization on the lumen. The promotion of the graft materials to the quick endothelialization in the lumen is of critical importance for vascular reconstruction. Furthermore, the incorporated growth of ECs and SMCs has been proven to be critical for successful grafting.[23] It is known that ECs affect abundant physiological processes, including thrombosis, platelet and monocyte activation/inhibition, SMC migration/proliferation and blood pressure.[24,25] On the other hand, SMCs are regarded as essential for functional vascular media engineering and for ECM deposition and remodeling.[24,26] Therefore, the challenge is always to encourage cell growth and tissue regeneration *in vivo* while maintaining patency and preventing acute thrombosis and restenosis in the application of tissue-engineered vascular grafts.[3,19]

Our previous study showed that in electrospun P(LLA-CL)–COL–CS composite scaffolds, well matched mechanical properties and optimal EC viability were reached, especially when the weight ratio of P(LLA-CL) to COL/CS was 3 : 1.[27] Based on such findings, further evaluation of the P(LLA-CL)–COL–CS scaffolds was conducted both *in vitro* and *in vivo*. Heparin was loaded into the grafts, using coaxial electrospinning for the inhibition of early thrombosis. *In vivo* patency of the grafts was compared by color Doppler flow imaging (CDFI) and digital subtraction angiography (DSA). Immunohistochemical analysis, collagen detection, RT-PCR, and western blot assay were conducted to systematically study the EC/SMC growth and vascular-related tissue reconstruction.

2. Experimental

2.1 Fabrication of P(LLA-CL)–COL–CS composite scaffolds

P(LLA-CL)–COL–CS composite scaffolds with ratios of 3 : 1 and 1 : 1 (w : w, P(LLA-CL) to COL/CS) were fabricated as previously described.[27] Briefly, P(LLA-CL) with 50% L-lactide (3×10^5 Da, Gunze Limited, Japan) and collagen type I (1×10^5 Da, Sichuan Ming-rang Bio-Tech Co., Ltd, China) were dissolved in 1,1,1,3,3,3-hexafluoro-2-propanol (HFIP, Fluorochem Ltd, UK), while chitosan (1×10^6 Da, 85% deacetylated, Jinan Haidebei Marine Bioengineering Co., Ltd, China) was dissolved in HFIP and trifluoroacetic acid (TFA, Sinopharm Chemical Reagent Co., Ltd, China) (v : v, 9 : 1) at concentrations of 8% (w/v). The COL/CS ratio in the blending solution was set at 4 : 1. Before electrospinning, P(LLA-CL) and COL/CS solutions were mixed at ratios of 3 : 1 (w : w) and 1 : 1 (w : w) and the grafts acquired were denoted as 3 : 1 and 1 : 1 composite grafts. A syringe pump (789100C, Cole-Pamer, Chicago, IL) and a high voltage power supply (BGG6-358, BMEICO, China) were used in the electrospinning process. The composite nanofibers were crosslinked for 48 h using glutaraldehyde vapor (GA, 25%, Sinopharm Chemical Reagent Co., Ltd, China) and stored in a vacuum-drying oven. Pure P(LLA-CL) scaffolds were fabricated as the controls.

2.2 Scaffold characterization

The morphology of the composite nanofibers was observed using Scanning electron microscopy (SEM) (JEOL JSM-5600, Japan). The chemical structure and composition of the nanofibers were characterized by Fourier transform infrared attenuated total reflectance spectroscopy (FTIR-ATR) (NEXUS-670, America). The suture retention strength with a 5–0 polyester suture (Shanghai Pudong Jinhuan Medical Products Co., Ltd, China) was tested by a micro material testing machine (MMT-250N, Shimadzu Co., Japan) using the reported methods.[28]

2.3 *In vitro* biodegradability

Different scaffolds were cut into rectangles (60 mm × 20 mm) for biodegradability tests within a scheduled time (150 days). The samples were placed in a phosphate buffered solution (PBS, pH = 7.2 ± 0.1) with sodium azide in a 37 °C water bath. SEM was used to observe morphological changes during the degradation process. The weight loss percentages were calculated using the following equation by the gravimetrical method:

$$\text{Weight loss } (\%) = \frac{W_0 - W_d}{W_0} \times 100\%$$

where W_0 is the initial weight and W_d is the dry weight after degradation. The pH value of the degradation solution was measured every month using a digital pH meter (PHS-3C, China). Three specimens were averaged for each sample.[29]

2.4 Cell viability and morphology

Human smooth muscle cells (hSMCs, purchased from the Institute of Biochemistry and Cell Biology, Chinese Academy of Sciences, China) were seeded on different electrospun scaffolds in 24-well plates at a density of 3×10^4 cells per well in 800 μL of Dulbecco's modified Eagle's medium (DMEM, Gibco Life Technologies Co., USA) with 10% fetal bovine serum and 1% antibiotic–antimycotic in an atmosphere of 5% CO_2 at 37 °C. After culturing for 5 days, 4′,6′-diamidino-2-phenylindole hydrochloride (DAPI, Invitrogen, USA) and rhodamine-conjugated phalloidin (Invitrogen, USA) were used to stain the nuclei and cytoskeletons of cells, and then the samples were observed using confocal laser-scanning microscopy (CLSM, Carl Zeiss LSM 700, Germany). The 3-(4,5-dimethyl-2-thiazolyl)-2,5-diphenyl-2*H*-tetrazolium bromide (MTT) assay was performed to test cell viability. After 1, 3 and 5 days of cell seeding, the cells and matrices were incubated with 5 mg mL^{-1} MTT for 4 h. 500 μL dimethyl sulfoxide (DMSO) solution was then used to dissolve the crystals. The UV absorbance values of 492 nm were measured using an Enzyme-labeled Instrument (Multiskan MK3, Thermo, USA). Mouse fibroblasts (L929 cells, purchased from the Institute of Biochemistry and Cell Biology, Chinese Academy of Sciences, China) were also seeded at a density of 1×10^4 cells per well under the same culturing conditions. Cell morphology was observed using CLSM after culturing for 5 days. Cell viability was measured by MTT assay after 1, 3, and 5 days.

2.5 Fabrication and characterization of heparin loaded vascular grafts

Heparin (1.3×10^4 Da, Runjie Chemical Co., Ltd, China) was dissolved in distilled water at a concentration of 15%. The heparin-loaded vascular grafts were fabricated using a custom-built electrospinning instrument with a coaxial setup. In the coaxial electrospinning process, heparin was injected at a flow rate of 0.2 mL h^{-1}, while the shell solution was injected at the rate of 1.0 mL h^{-1}. A rotating stainless steel mandrel collector (4 mm in diameter) was used to collect nanofibers. Heparin-loaded P(LLA-CL)–COL–CS vascular grafts were also crosslinked by GA vapor and stored in a vacuum-drying oven. FTIR-ATR measurement was performed on the grafts with heparin, and the suture retention forces were also tested as described in Section 2.2.

2.6 Implantation

Eight healthy Beagle dogs weighing 15–20 kg were used as the bilateral femoral artery replacement models in this study. All the experimental procedures involving animals in this study were conducted under institutional guidelines for animal care and approved by the Animal Ethics Committee of Shanghai Tenth People's Hospital (Shanghai, China). For each Beagle dog, the P(LLA-CL)–COL–CS–heparin vascular graft was implanted into the right femoral artery and the P(LLA-CL)–heparin vascular graft was implanted into the left one as control, as earlier described.[20] One dog was used for the autologous implantation.

Color Doppler flow imaging (CDFI) was performed continuously to observe the patency of the implanted grafts after 1, 4, 8 and 12 weeks. Digital subtraction angiography (DSA) was implemented to further compare the patency of different vascular grafts at 20 weeks. For the analyses of explanted grafts, the animals were killed humanely at 12 weeks by overdosed pentobarbital and the grafts were extracted.

2.7 Analyses of explanted grafts

2.7.1 Histological investigation. The cross-sectional segments of the implanted grafts were sliced and fixed with 4% paraformaldehyde and then cut into paraffin-embedded sections. Hematoxylin and eosin (H&E) staining was performed using conventional procedures. An immunohistochemistry assay with anti-von Willebrand factor (vWF, Abcam, UK) and anti-alpha-smooth muscle actin (α-SMA, Abcam, UK) was also performed on the sections. Then, biotin–streptavidin HRP Detection Systems (SP-9000, ZSGB-BIO, China) were incubated with the samples, followed by hematoxylin redyeing and observation with a light microscope.

2.7.2 Collagen detection. Representative paraffin sections of exposed grafts were dewaxed and then washed with distilled water. The samples were stained in 0.1% picrosirius red staining solution for 1 h and washed with distilled water for 5 minutes, followed by counter staining using Harris hematoxylin for dyeing nuclei. The samples were then dehydrated with gradient concentrations of ethanol and sealed using neutral balsam (Mounting Medium). The transparency of the samples was increased by xylene. The observation was performed under polarized light to identify collagen organization and maturation.[3] A hydroxyproline assay kit (Nanjing Jiancheng Bioengineering Institute, China) was used to evaluate the total collagen amount.

Table 1 The primer sequences for amplification

Gene/oligo name	Oligo sequence
Collagen I forward	5′-CCTGGAAGAGATGGTGCT-3′
Collagen I reverse	5′-CCATTCTTGCCAGCAGGAC-3′
Collagen III forward	5′-TGGCATTCCTCCGACTT-3′
Collagen III reverse	5′-CCATCCTCCAGAACTGTGTAT-3′
eNOS forward	5′-AGCCCGGGACTTCATCAATC-3′
eNOS reverse	5′-TGAAGCCGCTGCTCATGAG-3′
GAPDH forward	5′-TGGCGCTGAGTACGTCGTG-3′
GAPDH reverse	5′-ATGGCATGGACTGTGGTCAT-3′

2.7.3 Reverse transcriptase-polymerase chain reaction (RT-PCR). Total RNA was extracted using a total RNA extraction kit (Tiangen Biotech, China) and then RNA (1.0 μg) was reverse-transcribed into cDNA using M-MLV reverse transcriptase (Promega, USA). Expression levels of vascular related genes, including type I collagen (Collagen I, Abcam, UK), type III collagen (Collagen III, Abcam, UK), and endothelial nitric oxide synthase (eNOS, Abcam, UK), were detected by a PCR amplifier (FGEN02TD, Techne, UK). Glyceraldehyde 3-phosphate dehydrogenase (GAPDH) was used as an internal control and the primers are listed in Table 1. The PCR products were studied by 2% agarose gel electrophoresis. After checking RT-PCR products, the band intensities were measured and quantified using Image J software (National Institutes of Health, USA). All the measurements were performed in triplicate and the band intensity ratios were calculated by dividing the intensities of Collagen I, Collagen III, or eNOS by those of GAPDH.[30]

2.7.4 Western blot analysis. Cells and tissues on the explanted grafts were homogenized in lysis buffer and total proteins were collected by centrifuging at 10 000–140 000 rpm for 5 min (Thermo Fresco 17, USA). The total protein of the cell lysate was quantified by the BCA protein assay kit (Thermo, USA). Then, the total tissue protein was electrophoresed, transmembraned, and visualized by the conventional procedures of western blot.[31] The expressions of Collagen I, Collagen III, and eNOS in regenerated vascular tissues were detected with GAPDH as protein loading control.

2.8 Statistical analysis

Statistical analysis was performed using origin 8.0 (Origin lab Inc., USA). All the values were averaged at least in triplicate and expressed as mean ± standard deviation (SD). Statistical differences were determined by the analysis of One-Way ANOVA and differences were considered statistically significant at $p < 0.05$.

3. Results and discussion

3.1 Scaffold morphology

Fig. 1A displays the flow diagram of the electrospinning process for nanofibrous mats. The SEM images and fiber diameter distributions of pure P(LLA-CL) and 3 : 1 and 1 : 1 P(LLA-CL)–COL–CS scaffolds are shown in Fig. 1B and C. The composite scaffolds had nano-scaled structures with average diameters of

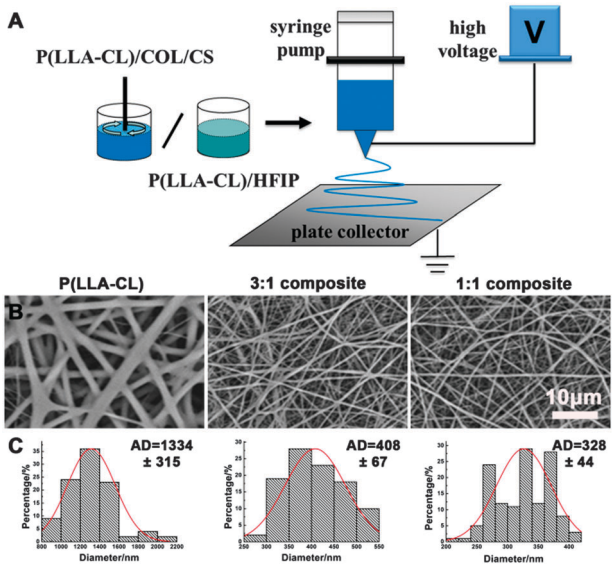

Fig. 1 (A) Diagram of electrospinning process for the fibrous mats. SEM images (B) and fiber diameter distributions (C) of the P(LLA-CL) and 3 : 1 and 1 : 1 P(LLA-CL)–COL–CS composite scaffolds.

408 ± 67 nm (3 : 1) and 328 ± 44 nm (1 : 1), while pure P(LLA-CL) fibers were of micro scale with an average diameter of 1334 ± 315 nm. As our previous study described,[27] the pure P(LLA-CL) scaffold had a larger pore diameter (2.2 ± 0.7 μm) than the 3 : 1 (1.1 ± 0.5 μm) and 1 : 1 (0.8 ± 0.4 μm) P(LLA-CL)–COL–CS scaffolds. These outcomes primarily resulted from the increased conductivity of the electrospinning solution with collagen and chitosan.[32]

3.2 Scaffold characterization

Collagen and polysaccharides are the main components of ECM, which possess high biocompatibility to promote cell adhesion and proliferation. For cell culture and further clinic application, composite scaffolds with collagen and chitosan were crosslinked using GA vapor to achieve an optimized crosslinking time (Table S1, ESI†). To determine whether the chemical structure of collagen and chitosan were altered after crosslinking, FTIR-ATR was utilized to analyze the characteristic absorption peaks of the amide groups and the diffraction peaks. It was found that the collagen and chitosan nanofibers maintained the characteristic groups of the original biomacromolecule (Fig. 2A). The characteristic absorption bands of collagen were observed at 1651 cm^{-1} (amide I), 1538 cm^{-1} (amide II), and 1201 cm^{-1} (amide III), while the peak at 1130 cm^{-1} was assigned to chitosan for its saccharine structure. The absorption peak at 3293 cm^{-1} was characteristic of –OH and –N–H vibrations.[33]

As a previous study showed, the composite scaffold with a ratio of 3 : 1 matched mechanical properties (tensile stress and elongation, burst pressure and dynamic compliance) with native blood vessels, but the 1 : 1 scaffold had a significantly lower ($p < 0.05$) tensile strength than the 3 : 1 composite scaffold.[27] This study further tested the suture retention force in the wet state (Fig. 2B). At the same thickness of 0.054 ± 0.001 mm,

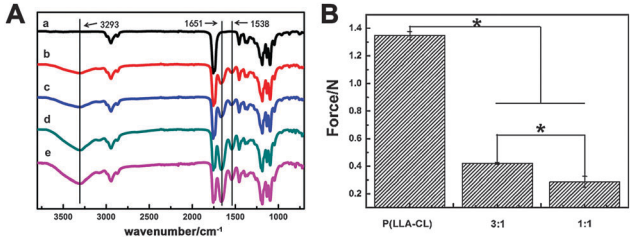

Fig. 2 (A) FTIR spectra of P(LLA-CL) (a), 3 : 1 (b, c), and 1 : 1 (d, e) composite scaffolds before crosslinking (a, b, d) and after crosslinking (c, e). (B) Suture retention forces of different scaffolds.

P(LLA-CL) nanofibers had the largest suture retention force (1.34 ± 0.03 N). Decreasing the proportion of P(LLA-CL) from 75% to 50% resulted in a decrease in the suture retention force from 0.42 ± 0.01 N to 0.29 ± 0.04 N. The mechanical properties demonstrated the potential application of 3 : 1 composite scaffolds in human blood vessels.

3.3 *In vitro* biodegradability

Fig. 3A shows the SEM micrographs of pure P(LLA-CL) and 3 : 1 and 1 : 1 composite scaffolds during the degradation process. Pure P(LLA-CL) nanofibers began to swell after 30 days of degradation. After 150 days, no fibrous morphology could be observed. However, fibers in 3 : 1 and 1 : 1 scaffolds presented distinct crimping and inter-bonding from the beginning of the degradation. The swelling and bonding of the fibers filled up the internal pores, and the fibrous morphology was barely observed from 30 days to 90 days. The swelling extent of the 3 : 1 scaffold was larger than that of the 1 : 1 scaffold, as more P(LLA-CL) was blended into the 3 : 1 scaffold. After degradation for 150 days, most fibers on the 3 : 1 composite surface lost their original morphology, but some fibers fractured on the 1 : 1 composite scaffolds with some crystal particles appearing on the surfaces because collagen and chitosan accounted for half of the amounts, and their crystalline region caused the breakage of fibers during the degradation.[29,34,35]

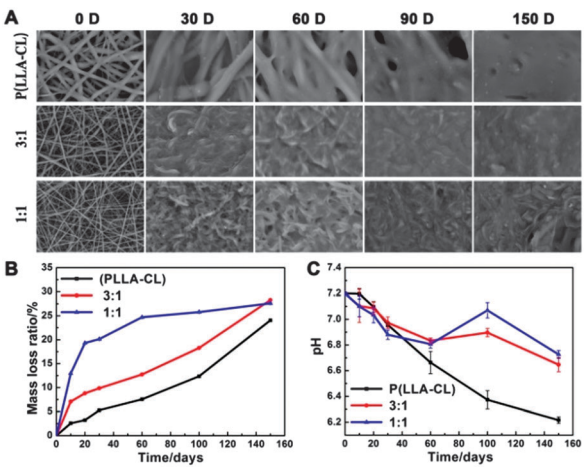

Fig. 3 (A) SEM images of the fiber morphology in P(LLA-CL) and 3 : 1 and 1 : 1 composite scaffolds during the degradation over 150 days. (B) The mass loss ratio. (C) The pH value change.

The mass loss ratio is shown in Fig. 3B. Pure P(LLA-CL) scaffolds had the lowest mass loss ratio of 24% after 150 days. This was mainly because the polymer chains in P(LLA-CL) were hydrolyzed to short chains but the degradation products of P(LLA-CL) were insoluble in PBS. In comparison, mass loss ratios of composite scaffolds were up to 28%, which could be attributed to the presence of hydrophilic COL/CS. The presence of hydrophilic material allows fast influx of water molecules and build-up of osmotic pressure within the matrix, resulting in a reduction of the lag phase.[36] Fig. 3C shows the pH value change at each time point. The pH value of pure P(LLA-CL) scaffolds kept decreasing during degradation, mainly because P(LLA-CL) was a block copolymer of PLLA and PCL and contained some acidic chain segments.[34] The pH values of 3 : 1 and 1 : 1 composite scaffolds fluctuated in a near-neutral range due to the neutralization of hydrolytic products from COL/CS.

3.4 Cell viability

The endothelial cells were found to proliferate and spread better on the 3 : 1 and 1 : 1 composite scaffolds than on pure P(LLA-CL) ones, mainly owing to the biological functional groups of collagen and chitosan.[27] In this study, the biocompatibility of relative cells, including SMCs and fibroblasts, were detected on the electrospun scaffolds (Fig. 4). Fig. 4A presents confocal microscopy photographs obtained after culturing for 5 days. hSMCs exhibited a better stretch on the composite nanofibers than on pure P(LLA-CL) scaffolds. The phenomenon became more apparent on the surface of the 3 : 1 scaffolds, where hSMCs were fully stretched into shuttle shapes. L929 cells showed faster growth on all the electrospun scaffolds than on hSMCs, but the cells were increasingly swollen with the addition of collagen and chitosan components. The proliferation rates of hSMCs and L929 cells on different scaffolds over 5 days are given in Fig. 4B and C. The results confirmed that the natural components in the composite scaffolds significantly promoted the proliferation of hSMCs and L929 cells compared to those on pure synthetic materials and coverslip controls, regardless of the culture time. The better cell growth may result from the higher specific surface area of the nanofibers and the functional reaction cues of collagen and chitosan.[37,38]

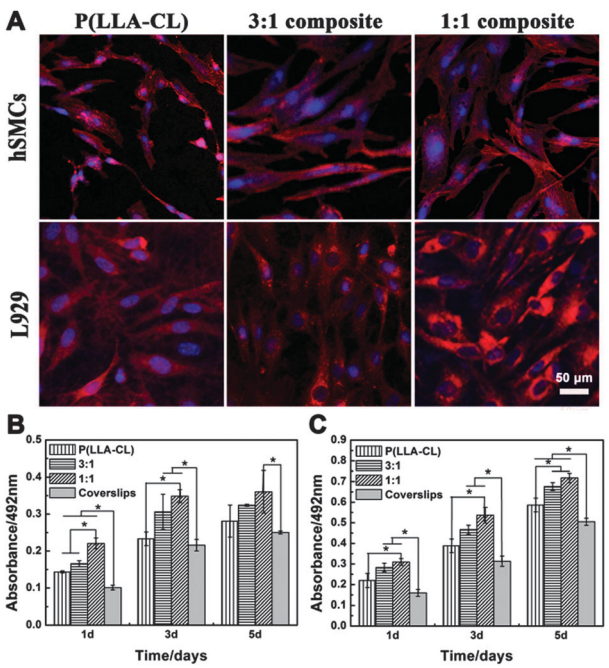

Fig. 4 (A) The confocal microscopy photographs of hSMCs and L929 cells after culturing for 5 days on the P(LLA-CL) and 3 : 1 and 1 : 1 composite scaffolds. Cell viability of hSMCs (B) and L929 cells (C) cultured for 1, 3, and 5 days.

3.5 Heparin loaded composite grafts *via* coaxial electrospinning

As can be seen from the above mentioned results, the 3 : 1 composite scaffolds had slightly lower cell viability but had significantly better mechanical properties than their 1 : 1 counterparts. Therefore, we selected 3 : 1 grafts for clinical tests. Heparin was added by coaxial electrospinning (Fig. 5A) to inhibit thrombosis and maintain patency in the earlier days after implantation. Fig. 5B and C are the microphotographs, SEM images and fiber distribution of the heparin loaded tubular grafts. The P(LLA-CL)–COL–CS–heparin and P(LLA-CL)–heparin tubular grafts, having an inner diameter of 3 mm and a length of 5 cm, were used for implantation. SEM images and fiber distribution analysis suggested a larger diameter for P(LLA-CL)–heparin fibers, as compared to P(LLA-CL)–COL–CS–heparin fibers. *In vitro* heparin release tests displayed that the coaxial electrospinning method could incorporate heparin in the scaffolds and that heparin release could be sustained for more than 20 days (Fig. 5D). FTIR spectra showed the typical absorption peak of heparin at 1640 cm^{-1}, caused by the –C═O stretching of the $–CONH_2$ group. The overlap of $–CONH_2$ in the range of 1640–1690 cm^{-1} could be attributed to the characteristic peak of both heparin and COL/CS in P(LLA-CL)–COL–CS–heparin grafts (ESI,† Fig. S1A). The suture retention strength of the P(LLA-CL) graft was larger than the P(LLA-CL)–COL–CS–heparin one, mainly because of its larger content of elastic P(LLA-CL) (ESI,† Fig. S1B).

3.6 Patency rate of the implanted grafts

Fig. 6A exhibits the surgical implantation of the electrospun vascular graft into the femoral artery of a Beagle dog. Fig. 6B shows the typical CDFI tracing images of the blood inflow into the arteries. Clear blood flow was observed that smoothly passed through the P(LLA-CL)–COL–CS–heparin tubular grafts after 1, 4, 8 and 12 weeks. The comparison of the patency in the left and right artery in one dog is shown in the DSA image (Fig. 6C). Blood flow was blocked when passing through the P(LLA-CL)–heparin graft, but it was able to pass through the P(LLA-CL)–COL–CS–heparin graft within 20 weeks. Based on the results of CDFI and DSA, patency rates at pre-determined time points are illustrated in Fig. 6D. The autologous artery showed a high patency of 100% until it was explanted for detection after 12 weeks. The P(LLA-CL)–COL–CS–heparin and P(LLA-CL)–heparin grafts expressed the same patency rate in the first 8 weeks after implantation (100% in 1 week, 85.7% in 4 weeks, and 57.1% in 8 weeks),

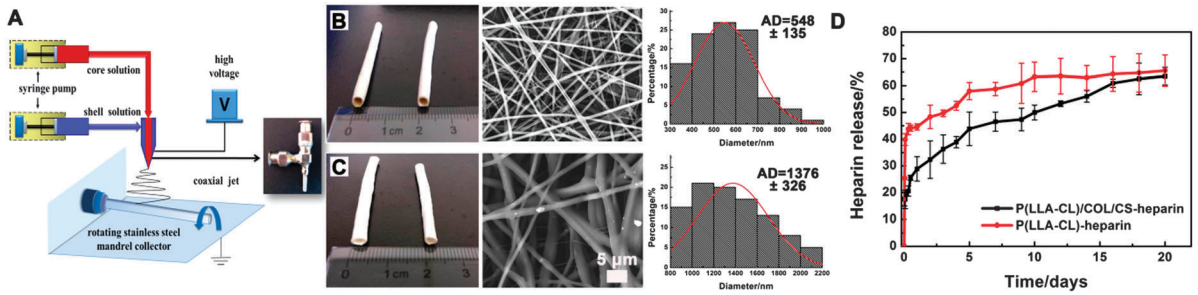

Fig. 5 (A) Schematic diagram of the electrospinning process used to fabricate the heparin-loaded grafts. (B, C) The digital photographs, SEM images and fiber distribution of the P(LLA-CL)–COL–CS–heparin graft (B) and P(LLA-CL)–heparin vascular graft (C). (D) Heparin release from P(LLA-CL)–COL–CS–heparin and P(LLA-CL)–heparin vascular grafts.

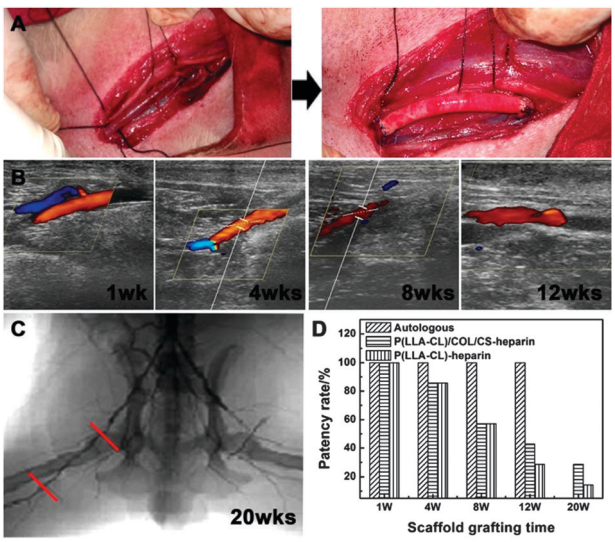

Fig. 6 (A) Surgical implantation of the electrospun vascular graft into the femoral artery of a Beagle dog. (B) The CDFI inspection of the P(LLA-CL)–COL–CS–heparin composite grafts at 1, 4, 8, and 12 weeks. (C) Typical DSA inspection of the P(LLA-CL)–COL–CS–heparin graft (right) and P(LLA-CL)–heparin graft (left) at 20 weeks. (D) Patency rates of various scaffolds after 1, 4, 8, 12, and 20 weeks of surgical implantation.

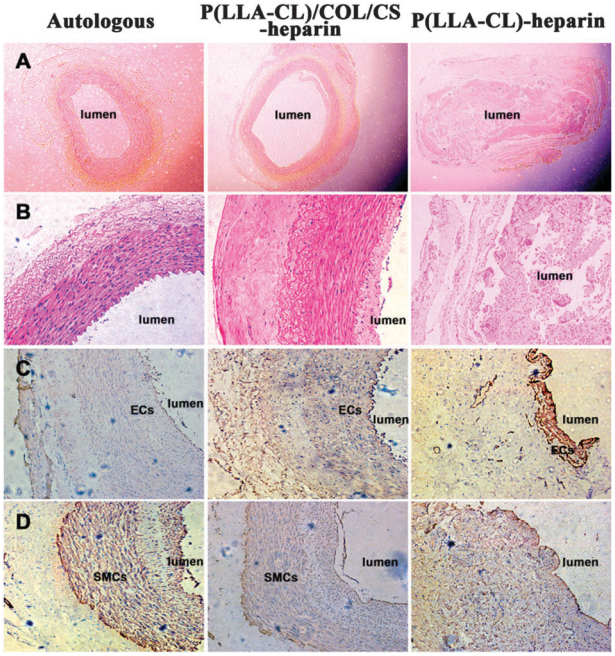

Fig. 7 (A and B) Typical H&E staining images (A: 40×; B: 200×) of the implanted grafts after 12 weeks. Immunohistochemistry images (200×) of vWF (C) and α-SMA (D) of the implanted grafts after 12 weeks.

owing to the anticoagulation effect from the released heparin in the early periods.[8] However, the P(LLA-CL)–heparin graft showed a poor patency rate after implantation for 12 weeks (28.6%) and 20 weeks (14.3%). In comparison, the P(LLA-CL)–COL–CS–heparin graft displayed higher patency (42.9% in 12 weeks and 28.6% in 20 weeks) than the P(LLA-CL)–heparin one, representing a better *in vivo* consistency.

3.7 Analyses of explanted grafts

3.7.1 Histological analyses. Fig. 7A and B present the H&E staining images of the implanted grafts at 12 weeks. The lumens of autologous and P(LLA-CL)–COL–CS–heparin grafts were fluent, while the P(LLA-CL)–heparin graft was blocked by blood clots. Magnified images in Fig. 7B show clear cell monolayers on the surface of both autologous and P(LLA-CL)–COL–CS–heparin grafts and some cells had infiltrated into the electrospun grafts. For the P(LLA-CL)–heparin graft, no cell growth or infiltration were observed. The immunohistochemical images of vWF and α-SMA further confirmed the results (Fig. 7C and D). In the autologous and P(LLA-CL)–COL–CS–heparin grafts, the endothelial cells grew effectively with a cell monolayer covering the entire luminal surface (Fig. 7C). On the contrary, only stacked cells were observed on the P(LLA-CL)–heparin surface. In Fig. 7D, regular and uniform SMC structures were detected in the autologous and the P(LLA-CL)–COL–CS–heparin graft, while no SMC structures were generated in the P(LLA-CL)–heparin group. These results showed that the endothelialization and SMC development on the P(LLA-CL)–COL–CS–heparin graft were highly matched with those of the autologous grafts, while pure P(LLA-CL)–heparin grafts had poor cell viability.

3.7.2 Collagen detection. The picrosirius red stained images of the explanted grafts are shown in Fig. 8 and the freshly generated collagen organization in the tissue was evaluated. Fig. 8A and B display the surrounding tissue with oriented structure (birefringent yellow/orange) in the autologous and

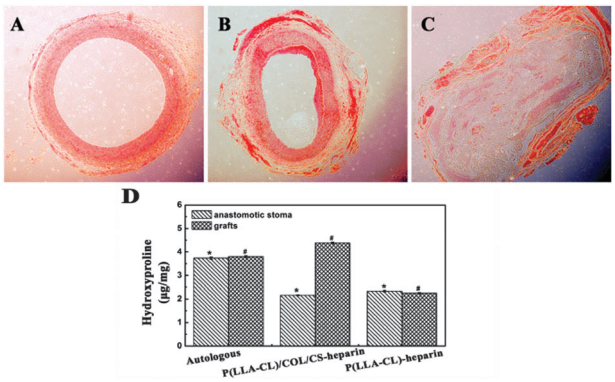

Fig. 8 Picrosirius red staining images of the autologous graft (A), the P(LLA-CL)–COL–CS–heparin graft (B) and the P(LLA-CL)–heparin graft (C) after 12 weeks. (D) Total collagen amount of the nearby anastomotic stoma and the implanted grafts.

P(LLA-CL)–COL–CS–heparin grafts, demonstrating the presence of mature Type I collagen fibers.[3,39] In comparison, the blocked P(LLA-CL)–heparin graft showed that considerably less collagen was present and the surrounding structure was random and indiscriminate (Fig. 8C). Calculation of the total collagen content using the conventional hydroxyproline assay, shown in Fig. 8D, further confirmed that the autologous and P(LLA-CL)–COL–CS–heparin grafts had higher collagen content than the P(LLA-CL)–heparin one with a significant difference of $p < 0.05$. The P(LLA-CL)–COL–CS–heparin graft even showed a higher collagen amount than the autologous graft, probably due to the collagen components being carried by the fibers themselves.

3.7.3 Relative gene and protein expression induced by P(LLA-CL)–COL–CS nanofibers. Collagen I, collagen III, and eNOS play important roles in the reconstruction of vascular related structures.[11,24,40] Based on the mRNA levels of collagen I, collagen III, and eNOS, the related gene expression of the remolding tissue on the explanted grafts was analyzed at 12 weeks through RT-PCR (Fig. 9A), and the band intensities were quantified and normalized to the expression level of GAPDH (Fig. 9C, D, and E). The collagen I expression levels of the autologous (0.96) and the P(LLA-CL)–COL–CS–heparin grafts (0.80) were significantly higher than that of the P(LLA-CL)–heparin graft (0.59). The nearby anastomotic stoma of the autologous graft (0.88) had a significantly greater collagen I expression than the other two groups (0.74 in P(LLA-CL)–COL–CS–heparin and 0.68 in P(LLA-CL)–heparin). Only the P(LLA-CL)–COL–CS–heparin graft and its anastomotic stoma had a comparable collagen I expression level.

For collagen III expression, the autologous graft showed no significant differences compared to its anastomotic stoma (0.91 in the autologous and 0.89 in the anastomotic stoma). However, collagen III was superiorly expressed on the P(LLA-CL)–COL–CS–heparin graft (1.07) compared to its anastomotic stoma (0.93), while the P(LLA-CL)–heparin graft showed an antipodal trend (0.92 in the graft and 0.99 in its anastomotic stoma). The eNOS expression level on each graft was comparable with that of the autologous graft, but the anastomotic stoma of the P(LLA-CL)–COL–CS–heparin graft expressed more eNOS than the P(LLA-CL)–heparin one ($p < 0.05$). The protein expression of collagen I, collagen III, and eNOS *via* western blot assay is presented in Fig. 9B. The collagen I and III expressions of both the autologous and the P(LLA-CL)–COL–CS–heparin

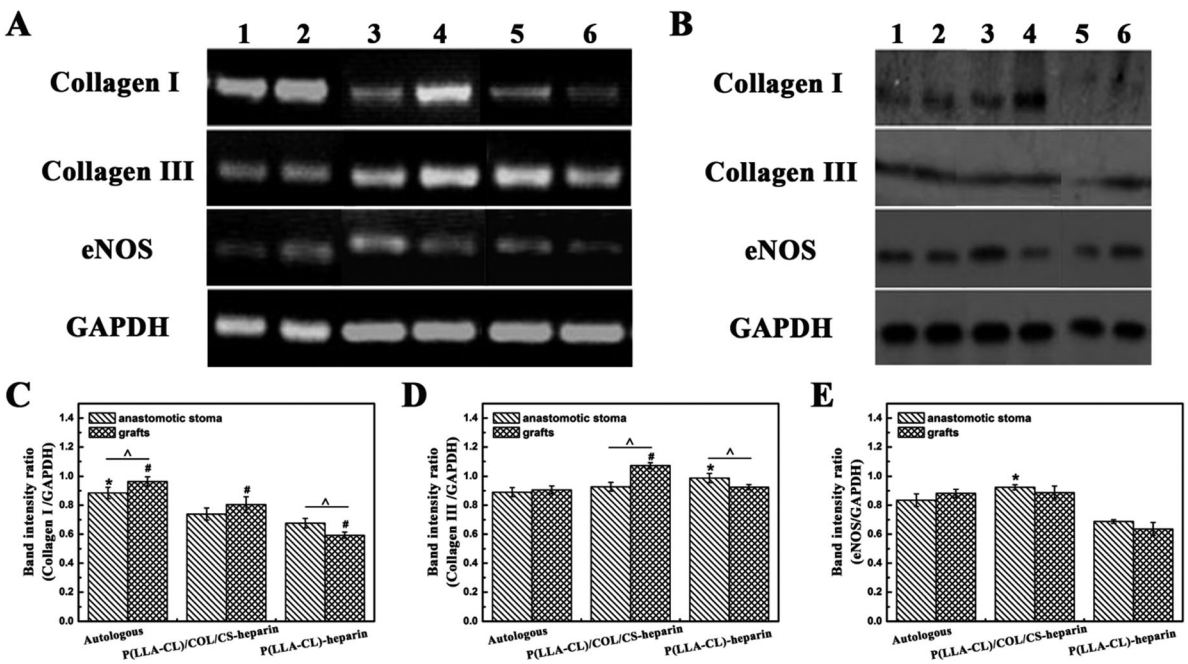

Fig. 9 mRNA expression levels (A) and western blot assay for the protein expressions (B) of collagen I, collagen III, and eNOS in the anastomotic stoma (1, 3, and 5) and grafts (2, 4, and 6) after 12 weeks (the autologous: (1, 2); the P(LLA-CL)–COL–CS–heparin graft: (3, 4); the P(LLA-CL)–heparin graft: (5, 6); GAPDH was used as loading control.). (C–E) Normalized expression levels of collagen I, collagen III, and eNOS mRNA with respect to GAPDH expression based on electrophoresis results.

graft were clearly observed, whereas the P(LLA-CL)–heparin graft had less collagen expression. The eNOS expression of each group was similar in general, except for the higher expression of the anastomotic stoma of the P(LLA-CL)–COL–CS–heparin graft, which confirms the results of RT-PCR. These results revealed that the combination of natural collagen and chitosan in the implanted grafts played a positive role in cell growth, ECM reconstruction and angiogenesis.

4. Conclusions

By adjusting the weight ratio of P(LLA-CL) and COL/CS to 3 : 1 in electrospun vascular grafts, we have found an optimal balance among mechanical properties, biodegradability and biocompatibility. *In vivo* studies further confirmed that the 3 : 1 composite graft possessed improved long-term patency and better development of ECs and SMCs, as well as enhanced vascular-related gene and protein expression in comparison to the pure P(LLA-CL) graft. Therefore, the 3 : 1 P(LLA-CL)–COL–CS composite scaffold provided important insight into the potential and development of biodegradable composite vascular grafts. Further cues could be integrated into the structure of such a matrix for the clinical application of *in situ* vascular tissue engineering.

Acknowledgements

This research was supported by the National Natural Science Foundation of China (31470941, 31271035, and 51403033), the Science and Technology Commission of Shanghai Municipality (11nm0506200), PhD Programs Foundation of the Ministry of Education of China (20130075110005), light of textile project (J201404) and the Fundamental Research Funds for the Central Universities (2232014D3-15).

Notes and references

1 C. K. Hashi, Y. Zhu, G.-Y. Yang, W. L. Young, B. S. Hsiao, K. Wang, B. Chu and S. Li, *Proc. Natl. Acad. Sci. U. S. A.*, 2007, **104**, 11915–11920.
2 J. Yu, A. Wang, Z. Tang, J. Henry, B. Li-Ping Lee, Y. Zhu, F. Yuan, F. Huang and S. Li, *Biomaterials*, 2012, **33**, 8062–8074.
3 M. Stoppato, H. Y. Stevens, E. Carletti, C. Migliaresi, A. Motta and R. E. Guldberg, *Biomaterials*, 2013, **34**, 4573–4581.
4 S. Shinohara, T. Kihara, S. Sakai, M. Matsusaki, M. Akashi, M. Taya and J. Miyake, *J. Biosci. Bioeng.*, 2013, **116**, 231–234.
5 M. J. McClure, D. G. Simpson and G. L. Bowlin, *J. Mech. Behav. Biomed. Mater.*, 2012, **10**, 48–61.
6 F. Han, X. Jia, D. Dai, X. Yang, J. Zhao, Y. Zhao, Y. Fan and X. Yuan, *Biomaterials*, 2013, **34**, 7302–7313.
7 H. Zhang, X. Jia, F. Han, J. Zhao, Y. Zhao, Y. Fan and X. Yuan, *Biomaterials*, 2013, **34**, 2202–2212.
8 Y. Yao, J. Wang, Y. Cui, R. Xu, Z. Wang, J. Zhang, K. Wang, Y. Li, Q. Zhao and D. Kong, *Acta Biomater.*, 2014, **10**, 2739–2749.
9 W. Fu, Z. Liu, B. Feng, R. Hu, X. He, H. Wang, M. Yin, H. Huang, H. Zhang and W. Wang, *Int. J. Nanomed.*, 2014, **9**, 2335–2344.
10 A. Perets, Y. Baruch, F. Weisbuch, G. Shoshany, G. Neufeld and S. Cohen, *J. Biomed. Mater. Res., Part A*, 2003, **65A**, 489–497.
11 S. A. Sell, M. J. McClure, K. Garg, P. S. Wolfe and G. L. Bowlin, *Adv. Drug Delivery Rev.*, 2009, **61**, 1007–1019.
12 K. von der Mark, J. Park, S. Bauer and P. Schmuki, *Cell Tissue Res.*, 2010, **339**, 131–153.
13 M. Z. Elsabee, H. F. Naguib and R. E. Morsi, *Mater. Sci. Eng., C*, 2012, **32**, 1711–1726.
14 Z. Wang, Y. Cui, J. Wang, X. Yang, Y. Wu, K. Wang, X. Gao, D. Li, Y. Li, X. L. Zheng, Y. Zhu, D. Kong and Q. Zhao, *Biomaterials*, 2014, **35**, 5700–5710.
15 S. de Valence, J. C. Tille, J. P. Giliberto, W. Mrowczynski, R. Gurny, B. H. Walpoth and M. Moller, *Acta Biomater.*, 2012, **8**, 3914–3920.
16 T. Pennel, G. Fercana, D. Bezuidenhout, A. Simionescu, T. H. Chuang, P. Zilla and D. Simionescu, *Biomaterials*, 2014, **35**, 6311–6322.
17 Y. Su, X. Li, Y. Liu, Q. Su, M. L. W. Qiang and X. Mo, *J. Biomater. Sci., Polym. Ed.*, 2011, **22**, 165–177.
18 R. Chen, C. Huang, Q. Ke, C. He, H. Wang and X. Mo, *Colloids Surf., B*, 2010, **79**, 315–325.
19 W. Zheng, Z. Wang, L. Song, Q. Zhao, J. Zhang, D. Li, S. Wang, J. Han, X. L. Zheng, Z. Yang and D. Kong, *Biomaterials*, 2012, **33**, 2880–2891.
20 C. Huang, S. Wang, L. Qiu, Q. Ke, W. Zhai and X. Mo, *ACS Appl. Mater. Interfaces*, 2013, **5**, 2220–2226.
21 M. Avci-Adali, G. Ziemer and H. P. Wendel, *Biotechnol. Adv.*, 2010, **28**, 119–129.
22 W. Wu, W. Yao, X. Wang, C. Xie, J. Zhang and X. Jiang, *Biomaterials*, 2015, **39**, 260–268.
23 N. L. James, K. Schindhelm, P. Slowiaczek, B. K. Milthorpe, N. P. B. Dudman, G. Johnson and J. G. Steele, *Artif. Organs*, 1990, **14**, 355–360.
24 N. Dahan, G. Zarbiv, U. Sarig, T. Karram, A. Hoffman and M. Machluf, *Tissue Eng., Part A*, 2011, **18**, 411–422.
25 M. D. K. K. Wu and M. D. P. Thiagarajan, *Annu. Rev. Med.*, 1996, **47**, 315–331.
26 L. Jiao, Z. Xu, F. Xu, S. Zhang and K. Wu, *Acta Cardiol.*, 2010, **65**, 499–506.
27 A. Yin, K. Zhang, M. J. McClure, C. Huang, J. Wu, J. Fang, X. Mo, G. L. Bowlin, S. S. Al-Deyab and M. El-Newehy, *J. Biomed. Mater. Res., Part A*, 2013, **101**, 1292–1301.
28 H. Bergmeister, C. Schreiber, C. Grasl, I. Walter, R. Plasenzotti, M. Stoiber, D. Bernhard and H. Schima, *Acta Biomater.*, 2013, **9**, 6032–6040.
29 K. Zhang, A. Yin, C. Huang, C. Wang, X. Mo, S. S. Al-Deyab and M. El-Newehy, *Polym. Degrad. Stab.*, 2011, **96**, 2266–2275.
30 J. S. Choi, K. W. Leong and H. S. Yoo, *Biomaterials*, 2008, **29**, 587–596.
31 Y. Yang, T. Xia, W. Zhi, L. Wei, J. Weng, C. Zhang and X. Li, *Biomaterials*, 2011, **32**, 4243–4254.
32 K. Zhang, H. Wang, C. Huang, Y. Su, X. Mo and Y. Ikada, *J. Biomed. Mater. Res., Part A*, 2010, **93**, 984–993.

33 C. Huang, R. Chen, Q. Ke, Y. Morsi, K. Zhang and X. Mo, *Colloids Surf., B*, 2011, **82**, 307–315.
34 Y. Dong, S. Liao, M. Ngiam, C. K. Chan and S. Ramakrishna, *Tissue Eng., Part B*, 2009, **15**, 333–351.
35 Y. Dong, T. Yong, S. Liao, C. K. Chan, M. M. Stevens and S. Ramakrishna, *Tissue Eng., Part A*, 2009, **16**, 283–298.
36 G. K. Jain, S. A. Pathan, S. Akhter, N. Ahmad, N. Jain, S. Talegaonkar, R. K. Khar and F. J. Ahmad, *Polym. Degrad. Stab.*, 2010, **95**, 2360–2366.
37 F. Tian, H. Hosseinkhani, M. Hosseinkhani, A. Khademhosseini, Y. Yokoyama, G. G. Estrada and H. Kobayashi, *J. Biomed. Mater. Res., Part A*, 2008, **84A**, 291–299.
38 M. Rafat, F. Li, P. Fagerholm, N. S. Lagali, M. A. Watsky, R. Munger, T. Matsuura and M. Griffith, *Biomaterials*, 2008, **29**, 3960–3972.
39 M. Ahmed, G. Hamilton and A. M. Seifalian, *Biomaterials*, 2014, **35**, 9033–9040.
40 U. Forstermann and T. Munzel, *Circulation*, 2006, **113**, 1708–1714.

